CONF-9506250-2

SLAC-PUB-95-6968
August 1995

Future High Energy Physics Experiments Using RICH Detectors: The Next Generation[1]

Blair N. Ratcliff

Stanford Linear Accelerator Center, Stanford University, Stanford, California, 94309, U.S.A.

Abstract

The physics goals and detector designs of high energy physics experiments now under construction that use RICH technology for particle identification are reviewed.

1 Introduction and Scope

This report describes some features of the new detectors now being constructed for use in high energy physics experiments that utilize RICH counters as a central element. Proposed experiments, and experiments in other areas, such as heavy ion physics or astrophysics, have been well-covered in other talks presented to this conference [1] and will not be included here. The scope of this discussion will be limited only to experiments which have been formally approved for construction as follows: (1) *BABAR* at PEP-II, which contains a quartz radiator DIRC counter; (2) CLEO III at the CESR upgrade, which utilizes a LiF/TEA Fast RICH; and (3) HERA-B at HERA, which uses a gas radiator RICH with either a TMAE- or a CsI-based photon detector. These experiments have much in common; all emphasize B-physics, run at the luminosity frontier, and plan to take first data either in 1998 or 1999.

This review will begin with a discussion of the physics goals and experimental context, and will then explore the designs which have been chosen to confront the experimental issues. Particular emphasis will be placed on the design and expected performance of the RICH detectors in these systems. Due to space limitations, only a few of the recent R&D results not covered elsewhere at the conference can be presented. Many more results have been presented at this conference [2]–[8], and these reports should be consulted for further details.

[1]Work supported by Department of Energy contract DE-AC0376SF00515.

Invited talk presented at the *International Workshop on RICH Detectors (RICH 95)* Uppsala, Sweden, June 12-16, 1995.

1.1 Physics Context

The apparent excess of matter over antimatter is one of the key puzzles requiring explanation in any description of the evolution of our universe. The Standard Model with three generations accommodates CP violation, but there is little direct evidence that its explanation is correct and, in any case, it is not complete. Attempts to explain the presently observed matter/antimatter imbalance of the universe with the Standard Model have not been successful, and further tests of the model are strongly indicated if they can be made.

It has been clear for a number of years that the study of CP-violating asymmetries in the decays of the B-meson system can, in principle, provide rigorous measurements of the parameters of the Cabibbo-Kobayashi-Maskawa (CKM) matrix and, in so doing, a stringent series of tests of the consistency of the Standard Model description of the CP-violation mechanism [9]. Thus, it is not surprising that a number of experiments have been proposed to confront this physics. These experiments use a variety of particle beams and energies, e.g., ranging from low energy e^+e^- machines operating at the $\Upsilon(4S)$, and experiments at the Z^0 pole, to hadronic experiments at the higher energies of HERA and LHC. From the detector perspective, all these experiments have a number of common requirements: (1) they need to reconstruct the CP eigenstates with high efficiency and low background; (2) they need to tag the flavor of the other B meson in the event; and (3) they need to measure the relative decay time of the two B-meson decays. As we shall see, these requirements lead to a number of common features for these experiments. In particular, high quality particle identification (PID) is crucial to solve requirements (1) and (2), and has thus been a major design goal of the experiments discussed below.

The more "classical" B-meson decay studies also can address many outstanding physics issues and are either made possible or greatly enhanced with high-quality PID, which improves the effective reconstruction efficiency and provides large improvements in signal-to-background. Typical examples include (1) the measurement of $b \to u$, e.g., in the decay $B^0 \to \pi^+\pi^-$; and (2) the measurement of CKM matrix elements, such as the ratio V_{td}/V_{ts}, using the $\rho\gamma$ to $K^*\gamma$ decay ratio. A panoply of other physics (e.g., charm, τ, and 2γ physics) also becomes accessible at the high luminosities of these machines, using good detectors with excellent PID.

1.2 The PID Environment

It is illustrative to provide a few specific examples of the way in which a good PID system confronts the required physics measurements. The discussion

below uses examples taken from the *BABAR* experiment [9], but are indicative of the relevant issues for both CLEO III [10] and HERA-B [11], once the different energies and operating environments are taken into account.

1.2.1 K Tagging

Tagging the flavor of the B mesons is crucial for the physics studies discussed above. A large enhancement in the efficiency of the tagging comes about if the kaon can be identified so as to tap the cascade chain $b \to c \to s$. As shown in Fig. 1, the kaon momentum spectrum is rather soft. The portion below about 700 MeV/c can be identified using ionization in the drift chamber. However, $\sim 40\%$ of the kaons lie at higher momentum where a dedicated PID system is necessary. The figure of merit is the effective tagging efficiency $\epsilon_{eff} = \epsilon(1-2w)^2$ where ϵ is the fraction of events tagged and w is the fraction of those in which the tag is of the wrong sign.

Table 1 shows the effect of a dedicated PID system on the kaon-tagging efficiency. The effective performance without such a system is poor and somewhat dependent on the dE/dx performance of the tracking detector. For the model used here, ϵ_{eff} is about 6% with very high wrong-sign tag rates. With perfect PID, assuming only decays in flight, the tagging efficiency using charged kaons alone is about 22%. After including information from the PID system of *BABAR*, the tagging efficiency remains nearly as high (about 20%) and is essentially independent of the detailed dE/dx performance of the tracker.

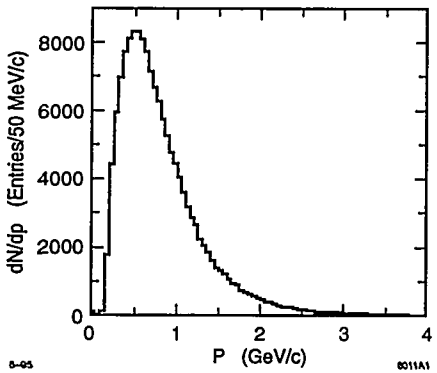

Fig. 1. Inclusive momentum spectrum for tagging kaons as a function of momentum in the laboratory frame.

Table 1
The tagging efficiencies (ϵ), the wrong sign rates (w), and the effective tagging efficiencies (ϵ_{eff}) for different levels of particle identification.

	ϵ(%)	w(%)	ϵ_{eff}(%)
Perfect Identification at Production	37	7	27
Perfect Identification with Decays	28	5	22
dE/dx Only	31	28	6
All PID	33	11	20

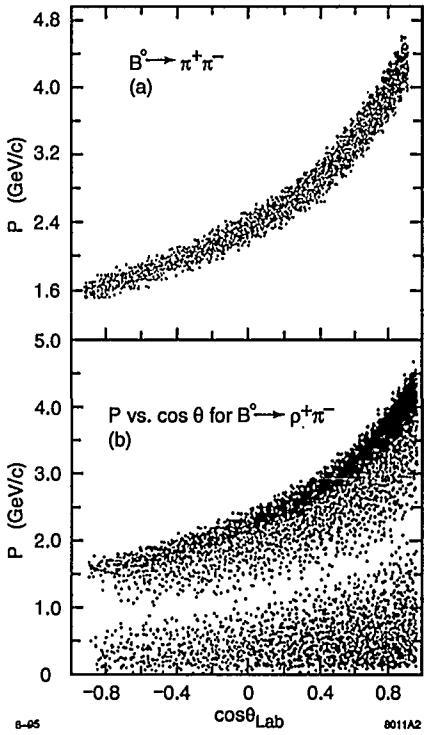

Fig. 2. (a) The momentum spectrum vs. the cosine of the laboratory angle for pions from the reaction $B^0 \to \pi^+\pi^-$. (b) The momentum spectrum vs. the cosine of the laboratory angle for charged pions from the reaction $B^0 \to \rho^+\pi^-$.

1.2.2 Exclusive State Reconstruction: The Measurement of sin 2α

The measurement of the CKM angle $\sin 2\alpha$ can be made using clean samples of the reactions $B \to \pi\pi$ and $B \to \rho\pi$ in all charge modes. Branching ratios are small and high reconstruction efficiencies must be obtained, while channels with kaons or K^* mesons must be rejected. The momenta are typically much

higher than those seen for tagging particles. The $\pi\pi$ final state, whose momentum spectrum is shown in Fig. 2(a), is the kinematically limiting reaction for B decays. It has a strong angle-momentum correlation due to the asymmetric environment of the machine with momenta exceeding 4 GeV/c in the forward direction. The $\rho\pi$ final state spectrum shown in 2(b) is bifurcated into low and high momentum portions, each of which are again strongly correlated with angle.

Figures 3(a) and 3(b) show the K/π separation performance obtained for the channels $B^0 \rightarrow \pi^+\pi^-$ and $B^0 \rightarrow \rho^+\pi^-$ respectively without a PID system (dashed line) and with a dedicated system (solid line). The ($\delta\chi^2$) rejection required depends on the background rejection requirements, but experience from past experiments would suggest a value somewhere in the middle of the range—perhaps 6-10. The performance without a PID system is clearly inadequate, with very low and rapidly varying reconstruction efficiencies for any separation, while with the DIRC-based system of *BABAR*, the performance is very good over a wide range.

2 *BABAR*

BABAR is the detector for the PEP-II machine at SLAC [9]. The primary goal of the expected 10-15 year experimental program is a complete series of measurements of the CKM matrix which elucidates the mechanism of CP violation and tests its description in the Standard Model. This full-scale program requires measurements of CP asymmetries in a wide variety of channels and measurements of branching fractions for a number of rare B meson decays. The machine is an asymmetric e^+e^- collider operating at 9 on 3.1 GeV, with a nominal initial luminosity of $3 \times 10^{33}\,\mathrm{cm}^{-2}\,\mathrm{s}^{-1}$. The experiment is also capable of performing next generation charm, τ, and 2γ experiments. The *BABAR* design is shown in Fig. 4.

Proceeding outward from the interaction region, *BABAR* consists of a silicon vertex detector to provide the precise location of the vertices and the track angles; a drift chamber to provide the primary measurement of the track momentum; a ring imaging DIRC counter to provide charged particle identification in the barrel, and a small two-layer aerogel threshold counter (ATC) to cover the forward endcap; a CsI electromagnetic calorimeter; and an instrumented flux return to identify muons and detect neutral hadrons. The detectors operate in a 1.5T field provided by a superconducting magnet. A summary of the performance parameters is given in Table 2.

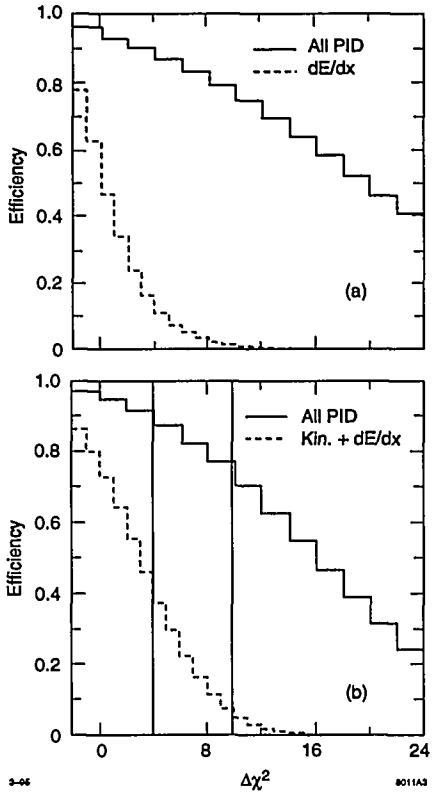

Fig. 3. The efficiency for accepting an event as a function of the χ^2 difference between events containing a $(\pi^+\pi^-)$ hypothesis and those containing a kaon; the dashed line shows the simulated performance without the PID system, while the solid line adds the DIRC and forward ATC systems of *BABAR*: (a) $B^0 \rightarrow \pi^+\pi^-$. (b) $B^0 \rightarrow \rho^+\pi^-$.

2.1 DIRC Design Issues

The DIRC detector [12] is designed to provide excellent particle separation performance for most ($\sim$ 92% of the tracking solid angle) tracks from B decays. Ionization loss in the tracking chamber gives good K/pi separation in the $1/\beta^2$ region below 700 MeV/c. The DIRC must therefore provide separation from 700 MeV/c up to the kinematic limit at about 4 GeV/c, taking into account the strong correlation between the lab angle and the momentum. It must also be robust and fast—insensitive to the noise that will be present in a high-luminosity environment. At the same time, it is important to take the minimum amount of radial space (8 + 1 cm on each side for clearance) so that the CsI volume and thus the overall detector cost can be minimized, and to place a minimum of material in front of the calorimeter ($\leq$ 18% X_0) so as not to degrade its low energy performance.

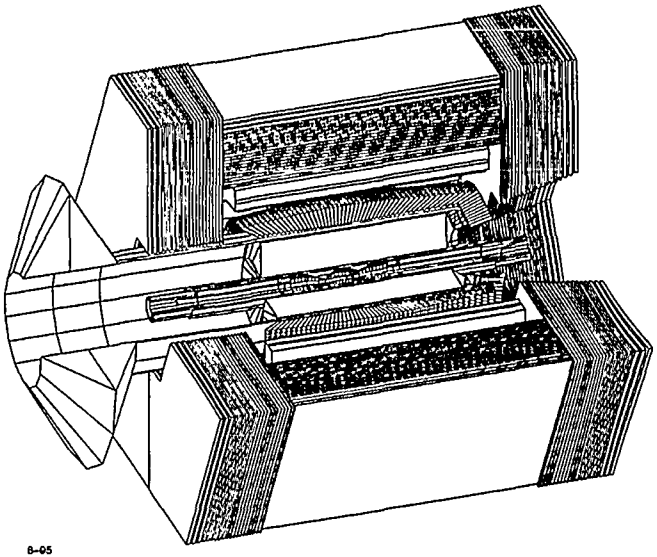

Fig. 4. A three-dimensional view of *BABAR*.

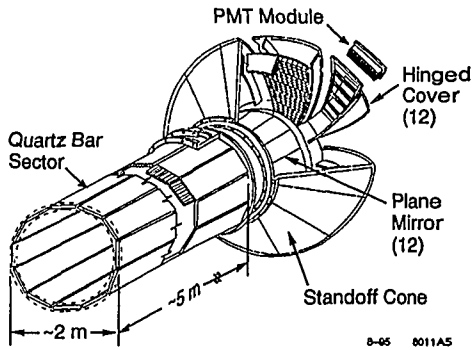

Fig. 5. A schematic showing the main elements of the DIRC.

The main elements of the DIRC design are shown in Fig. 5. The DIRC radiator consists of 156 quartz bars 1.75 cm thick, 3.5 cm wide, and 470 cm long, arranged in a 12-sided polygon around the beam line. This maximizes azimuthal coverage, simplifies construction, and minimizes edge effects. For sufficiently fast charged particles, some part of the Cherenkov radiation cone emitted by the particle ($\theta_c(E) = \cos^{-1}[1/\beta n]$), with $n = 1.474$) is captured by internal reflection in the bar and transmitted to the photon detector array located at the backward end of the detector. (Forward-going light is first reflected from a mirror located on the end of the bar.)

Table 2
Summary of the performance parameters for the *BABAR* systems (all angles are given in the laboratory [9]).

Detector	Technology	Dimensions	Performance
SVT	Double-Sided Silicon Strip	5 Layers $r = 3.2 - 14.4$ cm $-0.87 < \cos\theta < 0.96$	$\sigma_z = \sigma_{xy} = 50\mu\text{m}/p_t \oplus 15\ \mu\text{m}$ $\sigma_\phi = \sigma_\theta = 1.6\ \text{mr}/p_t$
DC	Small Cell Drift Chamber	40 Layers $r = 22.5 - 80.0$ cm $-111 < z < 166$ cm	$\sigma(p_t)/p_t = [0.21\% + 0.14\% \times p_t]$
PID	DIRC	1.75×3.5 cm^2 quartz $-0.84 < \cos\theta < 0.90$	$N_{pe} = 20 - 50$ $\geq 4\sigma K/\pi$ separation for all B decay products
PID	ATC	$n = 1.0065, 1.055$ $0.916 < \cos\theta < 0.955$	$N_{pe} = 10$ K/π separation up to 4.3 GeV/c
CAL	CsI(Tl)	$16 - 17.5\ \chi_0$ $\sim 4.8 \times 4.8$ cm crystals	$\sigma_{E/E} = 1\%/\text{E(GeV)}^{\frac{1}{4}} \oplus 1.2\%$ $\sigma_\theta = 3\ \text{mr}\ /\sqrt{E(\text{GeV})} \oplus 2\text{mr}$
MAG	Superconducting Segmented Iron	IR = 1.40 m L = 3.85 m	B = 1.5 T
IFR	RPC	16-17 Layers	$\epsilon_\mu > 90\%$ for $p_\mu > 0.8$ GeV/c

The high optical quality of the quartz bars preserves the angle of the emitted Cherenkov light. The measurement of this angle, in conjunction with knowing the track angle and momentum from the drift chamber, allows a determination of the particle velocity. An advantage of the DIRC at an asymmetric collider is that the high momentum tracks are boosted forward, which gives a much higher light yield than for particles at normal incidence. This is due to two effects: the longer path length in the quartz and a larger fraction of the produced light being internally reflected in the bar. The predicted K/π separation for the DIRC in *BABAR* is shown in Fig. 6 for the kinematically limiting reaction $B^0 \to \pi^+\pi^-$. Due to the increase in light yield for forward particles, the separation is essentially flat at about 4σ for the entire forward hemisphere, in spite of the strong momentum-angle correlation shown in Fig. 2(a). For other B-decay reactions, the track momenta are typically lower and the separation much larger.

The photon detector consists of about 13,000 conventional 1.125-inch-diameter phototubes. They are organized in a close-packed array at a distance of 120 cm from the end of the radiator bars. The phototubes, together with modular bases, are located in a gas-tight volume as protection against helium leaks from the drift chamber.

The photodetection surface approximates a partial cylindrical section in elevation and a toroid when viewed from the end. The standoff region has reflecting surfaces along the inner and outer radii to reduce the number of phototubes required. The opening angle between these surfaces is still under review but is taken to be 55° at this time. To maintain good photon transmission for all track dip angles, the standoff region is filled with water. The water seal occurs at a quartz window that is glued to the end of the bar assemblies. Most of the mass of the standoff box structure is high-permeability steel, which provides magnetic shielding for the phototubes.

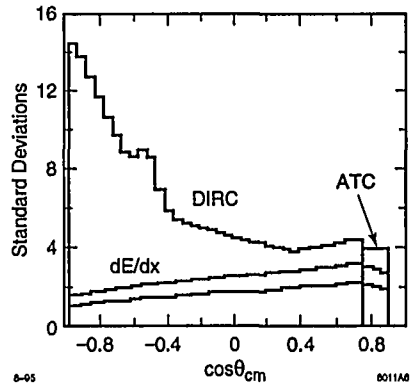

Fig. 6. The predicted K/π separation performance for the *BABAR* systems, in standard deviations versus the cosine of the center-of-mass polar angle, for pions from the reaction $B^0 \to \pi^+\pi^-$. The two curves labeled dE/dx indicate the range expected for separation using different models of the tracking chamber.

2.2 The DIRC Prototype Program

2.2.1 Prototype-I: Proof of Principle

The goal of the conceptual prototype (Prototype-I) was to demonstrate the basic proof of principle of the DIRC [13]. Because no detector like the DIRC had been built before, this prototype needed to address many fundamental issues and be easily modified to respond to new issues that arose during the studies. The detector was placed in a cosmic ray beam hardened to 1 GeV/c by an iron stack. A series of scintillation counters served as the trigger, and

a set of straw-tube chambers was used for tracking in the angular resolution studies. Quartz bars with sizes up to $240 \times 4.6 \times 1.7\,\mathrm{cm}^3$ were used, and a mirror was attached to the nonreadout end in order to make studies at an effective distance of 4 m from the readout end in the reverse configuration. Imaging was demonstrated with a small array of 47 EMI 9124A 29 mm photomultiplier tubes (PMTs) placed at varying distances from the end of the bar with air filling the standoff region, and other measurements were made into a Burle 8850 tube attached directly to the bar. A wide variety of studies were made to determine photoelectron yields and angular resolutions, as a function of track angle and bar position. Some examples of the results obtained are shown in Fig. 7. As reported fully elsewhere [13], these measurements were completed in 1994; were in agreement with Monte Carlo simulations based on the known optical, mechanical, and photoelectron detection properties of the components; and demonstrated the proof-of-principle for the device.

2.2.2 Prototype-II: Large-Scale Engineering Prototype

Prototype-II is a large-scale device which approximates a full-size section of the eventual configuration. It provides a realistic test bed for many of the principal engineering challenges and fundamental system performance issues in *BABAR*. In particular, it allows the observation of about 1/2 to 3/4 of a complete Cherenkov image, and the direct measurement of the particle separation, on a track-by-track basis. Moreover, because of its size, this prototype provides a realistic assessment of the impact of the mechanical structure on the performance of the final device. A short cosmic ray test of this device was successfully concluded in May 1995 [14], and the first tests of the device in a beam are underway at the time of this conference. Even though there have been few alignment or other studies done as yet, the results to date are very encouraging. A few very preliminary results from these tests will be given here, as no other report on these tests was given to this conference.

A cut-away isometric view of Prototype-II is shown in Fig. 8. The prototype consists of two 1.67 × 4.6 × 120 cm quartz bars glued together to form a composite bar 240 cm long. This bar is coupled to a water-filled standoff region with one mirror inside and 454 PMTs (29 mm in diameter) on the back plane of the standoff region for photodetection. The dimensions of the standoff box are 2.4 m wide by 1.2 m on each edge, with a 60° angle between each of the large surfaces. The phototubes are read out into standard modular electronics.

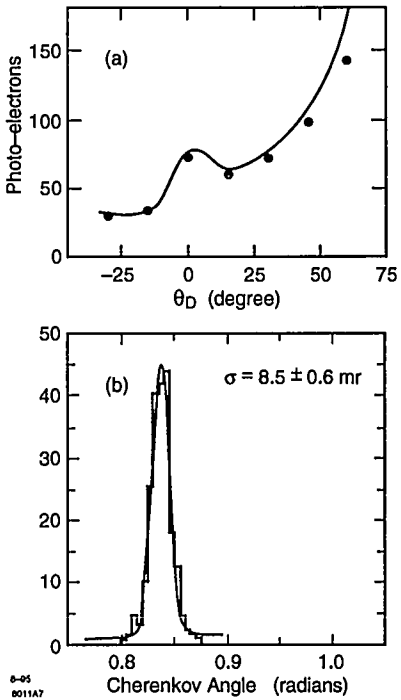

Fig. 7. (a) Observed photoelectron yield onto a single tube from a 1.7 cm-thick DIRC bar at a track position 60 cm from the photodetector end as a function of the track dip angle θ_D. The solid line is a Monte Carlo simulation; the statistical errors are smaller than the data points. There is a scale error of 3% due to calibration uncertainty. (b) Single Cherenkov photon angle distribution at $\theta_D = 30°$, a standoff distance of 90 cm, and a track position 205 cm from the end of a 240 cm-long bar. The line shows a fit to the data obtained with a Gaussian plus polynomial form.

An online display of a typical event obtained with a 5.4 GeV/c positive beam is shown in Fig. 9. The nine quartz back window panes are partially covered by 19 bundles with 24 PMTs per bundle as shown by the open circles. This arrangement of tubes is selected to accept track dip angles near ±20° for the run shown. The hit PMTs are shown as dark circles and form a clear "ring image."

The resolution obtained for tracks at a dip angle of 20° at a momentum of 5.4 GeV/c is shown in Fig. 10; Figure 10(a) shows the distribution function for the angular resolution per photoelectron obtained for particles tagged as pions by the beam line instrumentation. The resolution per photon is about 11.2 mrad, including a small misalignment systematic contribution. Figure 10(b) compares the average Cherenkov angle measured for particles tagged as pions

with those measured for particles tagged as protons. The separation shown is about 3.2σ; the distribution tails are very clean and essentially Gaussian.

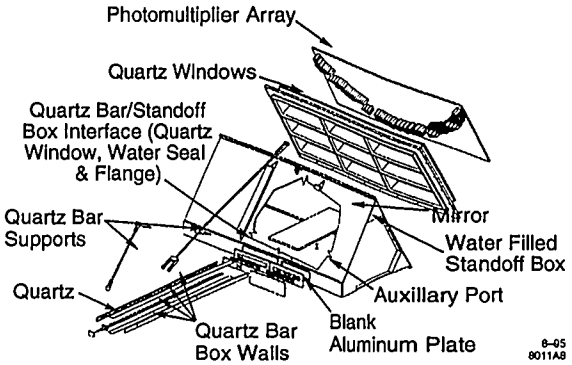

Fig. 8. Isometric view of the Prototype-II detector.

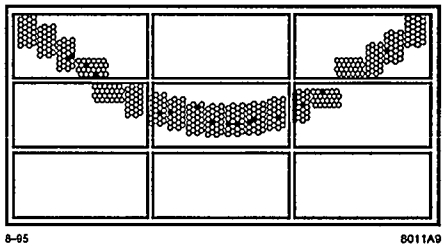

Fig. 9. Online display of a typical event in Prototype-II at a track dip angle of 20°.

Finally, Fig. 11 shows the measured average Cherenkov angle obtained as a function of momentum at a dip angle of 20° for tagged pions and protons. The curves give the expected angles for a quartz refractive index of $n = 1.474$.

3 CLEO III

CLEO III is an upgrade of the very successful CLEO II detector[10]. For the past several years, CLEO II utilized the large integrated luminosity provided by the CESR e^+e^- collider to perform high precision studies on many aspects of heavy flavor and τ physics. Over the next several year period, the CESR machine is being upgraded to provide integrated luminosities up to $15fb^{-1}$/year, providing an order of magnitude increase in the data. The gains from this increase in luminosity can be further enhanced by modifying the CLEO II detector. The detector with these upgrades, called CLEO III, has (1) improved vertex detection, and (2) a tracking system which maintains performance, while reducing space usage so that (3) a first-rate RICH PID system can be

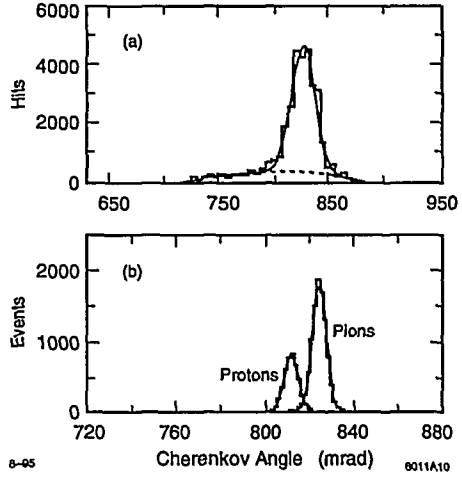

Fig. 10. Measured Cherenkov polar angles for (a) single photoelectrons from tagged pions; (b) average per track, for pions and protons.

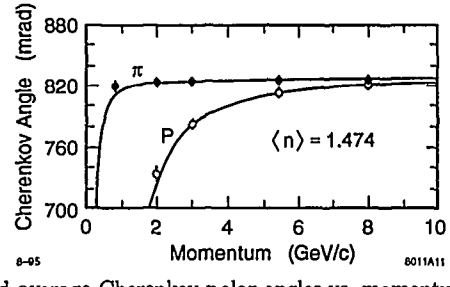

Fig. 11. Measured average Cherenkov polar angles vs. momentum for tagged pions and protons.

added. Taken in total, these upgrades should provide much cleaner data sets, make a variety of new topics accessible, and generally increase the effective number of reconstructed B mesons per unit of luminosity.

The primary goal of the expected program is to make a significant improvement in the B physics studies, particularly in the study of rare decay processes. It may also be possible to measure the Cabibbo-suppressed penguin decays such as $\rho\gamma$, and CP violation might be observed by measuring the rate of asymmetries in the decays $K^-\pi^+$ and $K^+\pi^-$. Finally, with the expanded data sets, much improved measurements of charm and τ decays will clearly be possible.

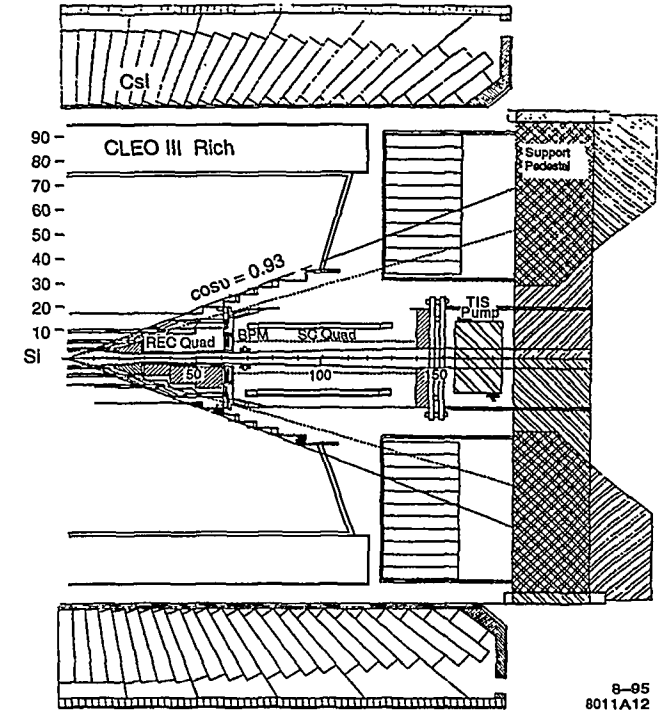

Fig. 12. An elevation view of one-half of the CLEO III detector.

The major elements of the CLEO III design are shown in Fig. 12. Proceeding outward from the interaction region, CLEO III consists first of a silicon vertex detector to provide the precise location of the vertices and the track angles. The resolution expected in the $r\phi$ plane is $\sigma \sim 10\mu$m, and $\sigma \sim 24\mu$m in Z. A drift chamber covering about 93% of the solid angle provides the primary measurement of the track momentum. The resolution performance is expected to be similar to that attained in CLEO II, i.e., $(\sigma_p/p)^2 = (0.0015p_t)^2 + (0.0056)^2$ for $p_t \geq 0.75$ GeV/c. A ring imaging LiF radiator fast RICH counter with a gaseous TEA photocathode provides excellent charged particle identification over the 80% of the solid angle that is covered by the barrel; K/π separation is expected at the 3.5σ level or better for momenta up to the kinematic limit for B decays (2.8 GeV/c). The CsI electromagnetic calorimeter should give resolution performance similar to that obtained in CLEO II; $\sigma_E/E = 0.0035/E^{0.75} + 0.019 - 0.001$E. A set of chambers is embedded in the flux return to identify muons. The detectors operate in a 1.5T field provided by a superconducting magnet.

3.1 *The LiF/TEA Fast RICH*

The components of the RICH detector [15] are illustrated in Fig. 13. The charged particles pass through a LiF solid radiator which is relatively transparent to the ultraviolet photons required to ionize TEA. Cherenkov photons are allowed to expand in a 16-cm-long expansion gap filled with Argon or Nitrogen gas. They travel through a CaF_2 window into a pad readout proportional chamber filled with methane gas with a small admixture of TEA to provide photosensitivity between 135 and 165 nm. The chamber anode pad gap is 1 mm and the pad area is 7.5×8 mm^2.

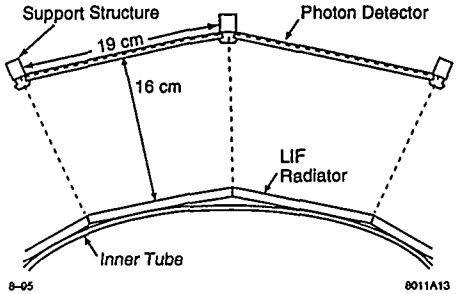

Fig. 13. A schematic end view of two sectors of the CLEO III Fast RICH detector. Not shown is the situation at polar angles near 90°, where the LiF radiators must be tilted by 20° to allow the Cherenkov cone to emerge with reasonable efficiency.

Estimates of the performance of this device are based on results obtained by the Fast RICH group at CERN [16]. This very similar prototype obtained an average of 10.4 photoelectrons at 25° yielding an overall resolution on the Cherenkov angle of 4.2 mrad per track. Since the K/π separation at 2.8 GeV/c is 12.8 mrad, a direct translation of these results implies $\sim 3\sigma$ separation—somewhat less than the goal of $\sim 4\sigma$. An extrapolation of these results based on a number of known problems and "features" of the CERN test prototype suggests that it should be possible to obtain substantially more photons (a predicted 43%) than seen in that test. These "features" include modest increases for fully covering the ring ($\sim$ 10%), instrumenting all the electronics ($\sim$ 5%), cleaning up the expansion gap gas ($\sim$ 5%), raising the chamber voltage onto plateau ($\sim$ 8%), and using thinner CaF_2 windows and strips ($\sim$ 8%).

A result of a Monte Carlo simulation of the predicted performance, taking 3/4 of this predicted increase, is shown in Fig. 14. The simulated K/π separation at 2.8 GeV/c is $\sim 3.5\sigma$, which is adequate for CLEO III, although falling slightly short of the 4σ goal.

It may be possible to use two additional features to improve the performance

still further. First, there is a correlation between conversion length in the proportional chamber and the wavelength of light which it may be possible to exploit if the chamber wires are instrumented with TDC readout. Since the chromatic term dominates the resolution for most angles, even a small improvement could be helpful. Second, as discussed earlier at this conference [3], alternative (sawtooth) radiators are being investigated which, if constructable, could significantly improve both the light yield and the photon resolution, albeit at the cost of more complicated images.

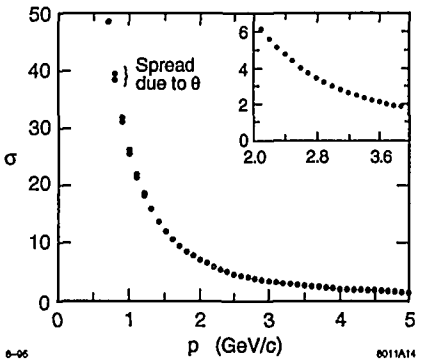

Fig. 14. Monte Carlo simulation of the K/π separation expected as a function of momentum for the Fast RICH at CLEO III. The spread in the points shows the separation range due to different values of the track polar angle. The inset shows the high momentum region magnified.

3.2 *The LiF/TEA Fast RICH Prototype Program*

The prototype program builds on the results obtained by the CERN Fast RICH group [2,16]. It includes small test chambers to study specific features of the gases and wire chamber geometries, full-length structures to look at mechanical issues, and a large single-ring prototype to do full-scale, ring-imaging studies, and test the electronics and operational features of the system design. Encouraging preliminary results from the single-ring prototype have been presented to this conference [7,8] that appear to validate most of the design assumptions of the group and give increased confidence that the calculated performance can be obtained in the CLEO III environment. The reader is encouraged to refer to these reports.

4 HERA B

HERA B is a dedicated B-physics experiment using an internal halo target located in the 820 GeV/c proton ring at HERA [11,17]. The main experimental goal is to make a definitive measurement of the CKM angle $\sin 2\beta$ using the channel $B \to J/\psi K_s^0$, where the $J/\psi \to \mu^+\mu^-$ and $K_s^0 \to \pi^+\pi^-$. The target is nondisruptive, and there is no significant interference with the other HERA operations. The experimental environment is in sharp contrast with the low production rate (but clean events) seen with the e^+e^- machines. Here the reactions of interest come from proton-nucleus collisions at 820 GeV/c. A typical event of interest contains a pair of b quarks, plus about ten other tracks and low-energy nuclear debris. However, such events are a very small fraction of all the events produced, which occur at the rate of about four events per beam crossing. The expected $b\bar{b}$ cross section is ~ 12 nb—less than 10^{-6} of the total cross section. Moreover, the ratio of the B events of primary interest to this experiment ($B \to J/\psi K_s^0$ decays) to all $b\bar{b}$ events is estimated to be about 4×10^{-6}. In short, the experimental environment is very challenging, having much in common with that expected at the very high energy hadron colliders such as LHC. Meeting these challenges requires a technically advanced detector that uses very powerful and efficient triggering and readout methods, and which has the ability to efficiently reject backgrounds. The major elements of the HERA B design are shown in Fig. 15.

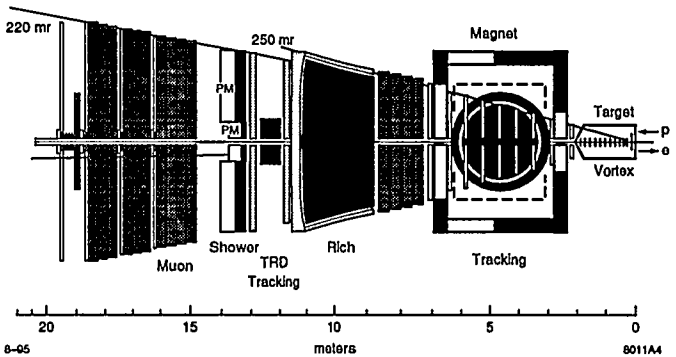

Fig. 15. Plan view of the HERA B detector.

Proceeding downstream from the interaction region, HERA B consists of a silicon vertex detector; a series of tracking chambers before and after a dipole magnet of 2.2 Tm; TRD and RICH counters for particle identification; an electromagnetic calorimeter; and a muon identification system. The solid angle ranges from 10 mrad to about 200 mrad, corresponding to about 90% of full coverage in the center of mass. Major emphasis in the design has been placed on: (1) the reconstruction of multiple events containing 50 to 100 tracks per beam crossing; (2) the efficient reconstruction of B-decay vertices with good

Table 3
Summary of the performance parameters for the HERA B systems.

Vertex detection	Impact parameter resolution:
	$\sigma \approx 25\ \mu$m $\oplus 30\mu$m$/p_t$ (in GeV)
	B vertex resolution:
	$\sigma_z \approx 500\ \mu$m, $\sigma_{x,y} \approx 25\ \mu$m
Magnetic analysis	Momentum resolution:
	$\Delta p/p \approx 2 \cdot 10^{-5} p \oplus 4 \cdot 10^{-3}$ (inner tracker)
	$\Delta p/p \approx 5 \cdot 10^{-5} p \oplus 5 \cdot 10^{-3}$ (outer tracker)
	Mass resolution:
	$\Delta M \approx 15$ MeV for $J\psi \to \mu^+\mu^-$
	$\Delta M \approx 8$ MeV for $B \to J/\psi K_s^0$ (constraint fit)
	$\Delta M \approx 23$ MeV for $B \to \pi^+\pi^-$
K/π separation	Momentum range ≈ 3 to ≈ 50 GeV
using RICH	$\pi \to K$ misidentification $< 2\%$ at $\approx 90\%$ K efficiency
e/hadron separation	Momentum range ≈ 1 to ≈ 70 GeV
using TRD	$h \to e$ misidentification $< 7\%$ at 98% e efficiency
EM calorimetry	Energy resolution:
	$\Delta E/E \approx 17\%/\sqrt{E} \oplus 1.6\%$ (inner)
	$\Delta E/E \approx 9.5\%/\sqrt{E} \oplus 1.0\%$ (middle and outer)
	Position resolution:
	$\Delta x, y \approx 1.2$ mm (inner)
	$\Delta x, y \approx 4$ mm (middle)
	$\Delta x, y \approx 10$ mm (outer)
e/hadron separation	$h \to e$ misidentification $\approx 3\%$ for $5 < p < 20$ GeV
using calorimeter	$\approx 1\%$ above 20 GeV
Muon identification	Momentum range > 5 GeV
	$\pi \to \mu$ misidentification $< 0.3\%$ at 30 GeV
	$K \to \mu$ misidentification $< 1\%$ at 30 GeV

resolution; (3) good lepton and kaon identification; (4) a fast, selective J/ψ trigger; and (5) resistance to radiation damage. A summary of the performance parameters expected for the detector components is given in Table 3.

Efficient tagging in HERA B requires the separation of kaons from pions and protons over most of the momentum acceptance of the experiment. These requirements are met by a fast RICH counter using a gas radiator and either a TMAE or CsI photocathode in a pad readout multiwire proportional chamber, as shown in Fig. 16. The optical system is folded to remove the photon detectors from the spectrometer acceptance. The six-meter focal length mirrors are similar to those used in the OMEGA RICH and can be constructed in a similar manner using hexagonal modules about 70 cm in diameter. The average point distortion is expected to be a bit less than 1 mm. The C_4F_{10} radiator is contained in an aluminum box. The 3 mm photon exit windows also serve as entrance windows for the photodetection chambers. C_4F_{10} is a transparent, stable "Freon" gas which does not deplete the ozone layer, and has been adopted by the SLD/CRID and DELPHI/RICH end caps. Its index of refraction ($n-1 = 1.5 \times 10^{-3}$) gives a Cherenkov angle of about 56 mrad for a $\beta = 1$ particle. The pad readout photon detectors are mounted as identical halves, above and below the magnet yoke. There are 64 chambers in all, each $\sim 50 \times 30$ cm^2. They are active over about 85% of the acceptance, and read out by electronics directly mounted on the chamber.

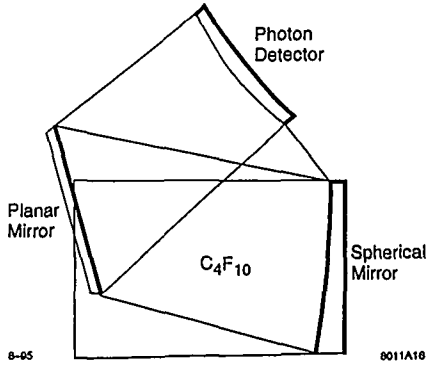

Fig. 16. Elevation schematic of one-half of the Fast RICH in HERA B.

The photocathode choice is still to be made. Two devices have shown promise in prototypes. The TMAE-based device, shown in Fig. 17(a), is similar in concept to the JETSET chambers. The 8×8 mm^2 cells, with 100-mm high, gold-coated bronze sheet walls, run at much lower TMAE concentrations than do DELPHI/RICH and SLD/CRID, thus reducing photon feedback. However, this cell geometry leads to a photon detection loss of $\sim$ 15% due to photons getting lost between the window and the active volume, or in hitting the bottom of the cell. A schematic of the CsI photocathode device geometry is shown in Fig. 17(b). The photons are detected by a reflective 1μm layer

deposited as 7.5×7.5 mm^2 pads on a metal surface. The 15 μm diameter anode wires are located 0.5 mm from the cathode pads and 1.5 mm from the 50 μm cathode wires.

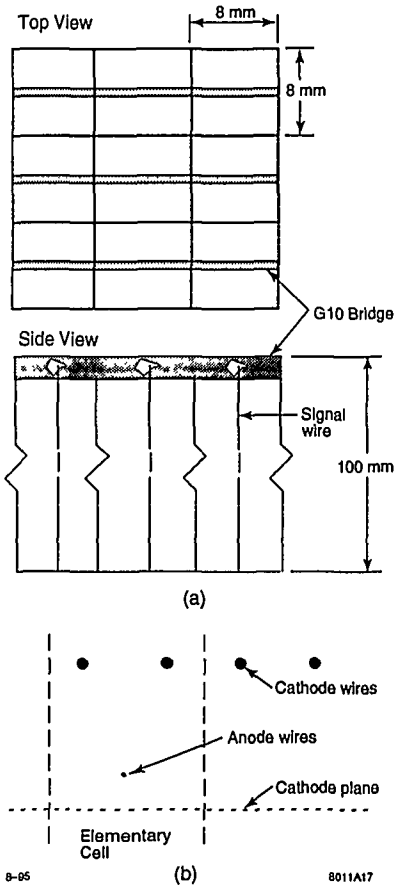

Fig. 17. Schematic views of the geometry of the photodetection chambers for the HERA B RICH: (a) with a TMAE photocathode, (b) with a CsI photocathode.

In general, the simulation uses parameters obtained from measured results. Approximately 57 and 51 photons are expected for the TMAE- and CsI-based detectors respectively. The angular resolution obtained per photon of 0.59 mrad is consistent with that observed by OMEGA RICH. For conservatism, 40 photoelectrons have been assumed in the calculations. In the absence of background, this would yield K/π separation of 3σ up to 80 GeV/c. However, there is significant event-correlated background coming particularly from

overlapping rings at small polar angles. This requires that the effects of this background be taken into account on an event-by-event basis using a reconstruction technique such as the maximum likelihood method. The expected performance obtained for this device is shown in Fig. 18.

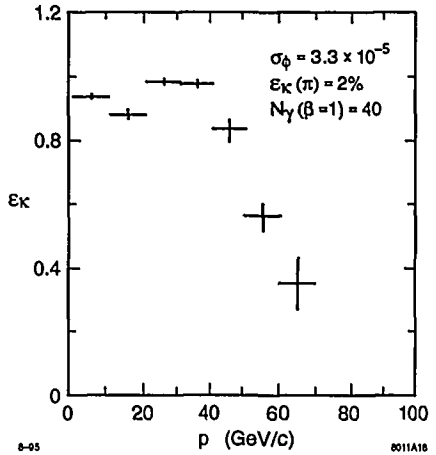

Fig. 18. Momentum dependence of the kaon detection efficiency for a fixed 2% pion fake probability.

4.2 The HERA B RICH Prototype Program

A program of prototype tests is underway to validate the performance assumptions used and ensure that the devices are sufficiently robust. These tests include extensive studies of photon detector aging rates using a UV light source, studies of detector replacement scenarios, and the measurement of the transmission of the C_4F_{10} radiator. Recently, highly successful beam tests of a prototype RICH system have been performed with both TMAE- and CsI-based detectors in a 3 GeV/c electron beam at DESY. These results have been reported in detail to this conference [5,6], and the reader is encouraged to refer to these reports. These tests used an argon radiator, and two different chambers (one CsI and one TMAE) were illuminated by the ring. The TMAE-based device was very reliable and stable from the beginning, while the CsI chamber operated successfully after initial problems. However, its efficiency was not uniform. Both devices gave similar resolution performance in the optimum regions. However, the CsI detector gave about 60% of the photon yield observed by the TMAE detector. The reasons for this are under study. The final choice of detector type is expected to be made this summer (1995) based on the results of the aging and high rate tests.

5 Summary

Highly efficient, robust PID systems are required for the second generation B physics experiments now being constructed. First data are expected in 1998 with CLEO III and HERA B, and in 1999 with *BABAR*. A new generation of RICH detectors have been designed which are able to match the performance needs in the high luminosity environment of these experiments. Large-scale prototype work is underway on these systems and results are very encouraging. However, the time scales are extremely short, and construction must be started soon to meet the required construction schedules. Overall, RICH devices should play a major role in several of the most interesting and fundamental experiments to be performed in high energy physics in the next decade, and the future looks bright for the RICH technique as we head into the next century.

References

[1] See, for example, the reports to this conference by C. Speiring, and E. Nappi.

[2] J.L. Guyonnet et al., report to this conference.

[3] S. Stone et al., report to this conference.

[4] C. Mindas et al., report to this conference.

[5] T. Hamacher et al., report to this conference.

[6] M. Staric et al., report to this conference.

[7] S. Playfer et al., report to this conference.

[8] M. Artuso et al., report to this conference.

[9] See, for example, the *BABAR* Collaboration, "*BABAR* Technical Design Report," 40, SLAC-R-95-457 (1995).

[10] The CLEO III Collaboration, "The CLEO III Detector: Design and Physics Goals," CLNS 94/1277 (1994).

[11] The Hera-B Collaboration, "HERA-B: An Experiment to Study CP Violation in the B System Using an Internal Target at the HERA Proton Ring," DESY-PRC 95/01 (1995).

[12] B. Ratcliff, *BABAR* Note 92, and SLAC-PUB-6047 (1993), published in Tsukuba B Factories, 331-341 (1992); P. Coyle et al., "The DIRC Counter: A New Type of Particle Identification Device for the B Factory," Nucl. Inst. and Methods **A343**, 292 (1994).

[13] D. Aston et al., "Test of a Conceptual Prototype of a Total Internal Reflection Cherenkov Imaging Detector (DIRC) with Cosmic Muons" SLAC-PUB-6731 (1994).

[14] R. Aleksan et al., the DIRC Collaboration of *BABAR*.

[15] M. Artuso et al., HEP 94-7 (1994).

[16] J. Seguinot et al., Nucl. Inst. and Methods **A350**, 430-463 (1994).

[17] P. Krizan et al., Nucl. Inst. and Methods **A351**, 111 (1994).